Rectifying Acoustic Waves

S. Shirota, Ramya Krishnan, Y. Tanaka, and N. Nishiguchi*
Department of Applied Physics, Hokkaido University, Sapporo 060-8628, Japan
(Dated: June 22, 2007)

We propose a system to rectify acoustic waves. The system comprises of an array of triangular holes drilled in an elastically isotropic material. Assuming propagation of transverse acoustic waves with polarization parallel to the holes, we confirm numerically that rectification of acoustic waves occurs even in the frequency region with corresponding wavelength comparable to the dimensions of the scatterers. The rectification effects appear above a threshold frequency due to the Bragg diffraction owing to the periodic structures. The threshold frequency depends on structural parameters, which enables to realize a tunable rectifier.

PACS numbers: 43.20.Gp,73.40.Ei,62.65.+k

Rectification is an essential function of electronic devices, and recent studies of geometric effects on the transport in the nano structures revealed that asymmetric scatterers such as triangular potential barriers give rise to rectification of electrons[1–4], superconducting vortices[5] and thermal solitons[6]. Although the geometric effects are confirmed only for the ballistic-particle flows, we can also expect the geometric effects on rectification of acoustic-wave propagation in the very short wavelength limit. In the extreme case, the wave propagation can be illustrated in terms of ray-acoustics, and specular reflections of the rays from the surface of scatterers govern the transmission through the scatterers. Considering case (I) that rays incoming from the left region toward a matrix with equilateral-triangular ($\alpha = \frac{\pi}{3}$) holes of periodically aligned in the y-direction as shown in Fig. 1, one half of them are scattered backward, and the rest passes between the scatterers. The resultant transmission rate becomes 0.5, where the neighboring holes are uniformly spaced by the same distance as the base of a triangular void. On the other hand, the transmission rate becomes 1 for case (II) where the rays impinge on the summits of the triangular voids from the right region, since the rays reflected from the surface are transmitted to the left region through the passes between the holes. Thus the acoustic waves are rectified in the very short wavelength limit.

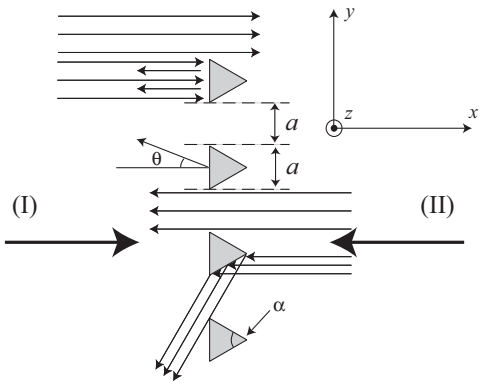

FIG. 1: z-polarized transverse acoustic wave reflection from isosceles-triangular holes of angle α drilled in an elastically isotropic material. The triangles are separated by the same distance as the base, and are aligned in the y direction. The thick arrows indicate the directions (I) and (II) of incident waves. The thin arrows show reflection and transmission of waves in the very short wavelength limit, where the diffraction is ignored.

The prediction by the ray-acoustics cannot be immediately applied to the wave propagation at finite wavelength because of a decay in the geometric effects and of interference effects. Generally speaking, the larger the wavelength becomes, the less important the geometric effects on wave propagation will be, in particular, for the wavelength comparable or larger than the dimensions of scatterers. The waves peculiar to the geometry of scatterers decay near the scatterers and only the azimuthally symmetric waves propagate in the asymptotic field as a cylindrical wave in a two-dimensional (2D) system or a spherical wave in a 3D one, where interference among the scattered waves will dominate the wave propagation as discussed in photonic and/or phononic crystals. These considerations lead to gradual decay and vanishing of the rectification effects with increasing wavelength. In addition, the perturbation theory based on the Rayleigh scattering does not lead to the rectification of waves. From these considerations, the rectification seems hopeless for finite wavelength.

In the present work, we show that the rectification effect vividly survives even in the frequency region with corresponding wavelength comparable to the dimensions of the scatterers, and that, in spite of the conjecture, there is a threshold frequency, below which rectification does not take place at all. Very interestingly, the threshold frequency stems from the Bragg diffraction due to the structural periodicity of scatterers, indicating that the rectification effects are tunable by adjusting the arrangement of the scatterers.

The system to be studied is an elastically isotropic material containing one-dimensional array of isosceles-triangular holes with summit angle α in the y direction,

whose axis is in the z direction as shown in Fig. 1. The distance between the neighboring triangles is the same as the base length of the triangles. The holes are left empty in order to get strong reflection of acoustic waves, irrespective of frequency.

Considering z-polarized transverse acoustic (TA) waves propagating in the $x-y$ plane, we ignore complicate mode conversions among longitudinal acoustic (LA) and TA waves. The equation of motion for the z-component of displacement u_z becomes a scalar wave equation with sound velocity c

$$\left(\nabla^2 - \frac{1}{c^2}\partial_t^2\right) u_z = 0. \tag{1}$$

We employ free surface boundary condition at the surface of the scatterers. By means of a Finite-Difference Time-Domain (FDTD) method[7], we numerically simulate the wave propagation across the scatterers. We actually investigate the wave propagation in a thin slip of width of $2a$ using periodic boundary condition in the y direction because of the periodic arrangement of the scatterers in this direction. We use 2nd-Mur absorption boundary condition[8] for the ends of the slip so that the reflected waves from the ends of the slip are not contained for energy flow detection.

The incident waves impinge perpendicularly to the array of scatterers, and we investigate the difference in the transmission rates between the incident directions (I) and (II). The Poynting vector in the present system is defined from the continuity of energy flow as $\mathbf{J} = -\dot{u}_z(\sigma_{zx}, \sigma_{zy}, 0)$, where $\sigma_{z\alpha}$ is the stress tensor defined by $\sigma_{z\alpha} = \mu\partial_\alpha u_z$. Here μ is one of the Lamè constants. The total energy flow is described in terms of the Fourier components of the displacement $\hat{u}_z(\omega)$ and the stress tensor $\hat{\sigma}_{z\alpha}(\omega)$ as

$$\int_{-\infty}^{\infty} \mathbf{J}dt = -4\pi \mathrm{Im}\left[\int_0^{\infty} \omega \hat{u}_z(\omega)(\hat{\sigma}^*_{zx}(\omega), \hat{\sigma}^*_{zy}(\omega), 0)d\omega\right], \tag{2}$$

and the contribution at ω, $\hat{\mathbf{J}}(\omega)$, to the total energy flow reads

$$\hat{\mathbf{J}}(\omega) = -4\pi \mathrm{Im}[\omega \hat{u}_z(\omega)(\hat{\sigma}^*_{zx}(\omega), \hat{\sigma}^*_{zy}(\omega), 0)]. \tag{3}$$

Here $\mathrm{Im}[A]$ means the imaginary component of A. We define the transmission rate $T(\omega)$ by the ratio of the x-component of $\hat{\mathbf{J}}(\omega)$ integrated over the $y-z$ plane to that in the absence of scatterers, where the latter is distinguished by a superscript 0;

$$T(\omega) = \left.\frac{\int \hat{J}_x(\omega)dydz}{\int \hat{J}^0_x(\omega)dydz}\right|_{x=x_D}. \tag{4}$$

Although the detecting position x_D is put $x_D = 3a$ from the scatterers in their right side for case (I), and in the left side for case (II), the transmission rate is, of course, independent of x_D.

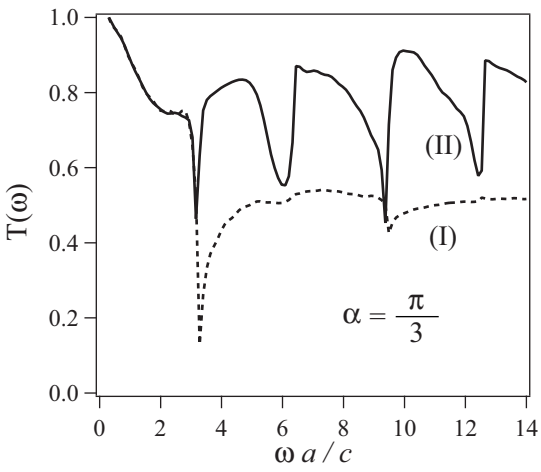

FIG. 2: Transmission rate versus frequency for $\alpha = \frac{\pi}{3}$. The dashed and solid lines indicate the transmission rate for case (I) and (II), respectively.

Figure 2 shows the transmission rates versus frequency in case of $\alpha = \frac{\pi}{3}$ for two different incident directions (I) and (II). The two transmission rates coincide for $\frac{\omega a}{c} < \pi$, and they show distinct dependences on frequency for $\frac{\omega a}{c} > \pi$; the transmission rate for (I) shows periodic changes with period $\frac{\Delta\omega a}{c} = \pi$ around $T = 0.5$ with increasing frequency. The transmission rate for (II) also shows periodic change with the same period as (I), however, whose average magnitude and amplitude are much larger than those for (I). The obvious difference in the transmission rates above $\frac{\omega a}{c} = \pi$ between (I) and (II) indicates that the rectification takes place at wavelength comparable to the dimension of the scatterers, i.e $\frac{a}{\lambda} > \frac{1}{2}$, considering the linear dispersion relation $\omega = kc = \frac{2\pi c}{\lambda}$. The periodic behavior of the transmission is characterized by the dips, which appear when $\frac{\omega a}{c} = n\pi$. Hereafter n indicates an integer. Interestingly, the dips at $\frac{\omega a}{c} = \pi$ and 3π are more prominent than those at 2π and 4π, which will be discussed below. The properties of the transmission rates shown in Fig. 2 are not unique to the equilateral-triangular holes($\alpha = \frac{\pi}{3}$), but the characteristic properties of rectification are also found in case of isosceles-triangular holes. Figure 3 shows the transmission rates versus frequency for $\alpha = \frac{2\pi}{9}$, where the distance between the holes are the same as the base of the isosceles triangle. The rectification, the periodic changes in the transmission rates of period π and the threshold frequency are also found in this case. In particular, the transmission rates for (II) of $\alpha = \frac{2\pi}{9}$ are larger than those for $\alpha = \frac{\pi}{3}$, which shows the rectification is enhanced with decreasing α.

Within the ray-acoustics approximation, the transmission rate of case (II) is 1 for $\alpha \leq \frac{\pi}{3}$ and 0.5 for $\alpha \geq \frac{\pi}{2}$, and varies as $T = \frac{1}{2} + \cos\alpha$ for $\frac{\pi}{3} < \alpha < \frac{\pi}{2}$. On the other

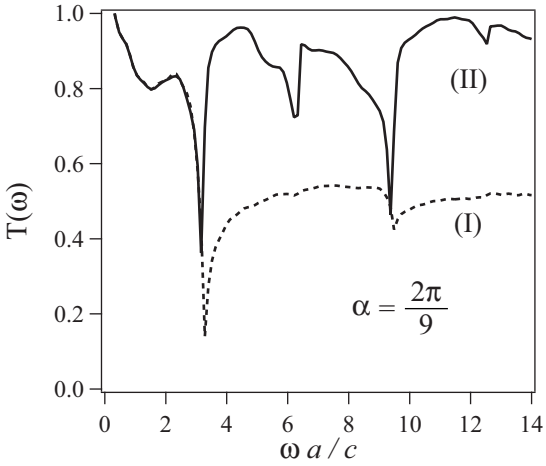

FIG. 3: Transmission rate versus frequency for $\alpha = \frac{2\pi}{9}$. The dashed and solid lines indicate the transmission rate for case (I) and (II), respectively.

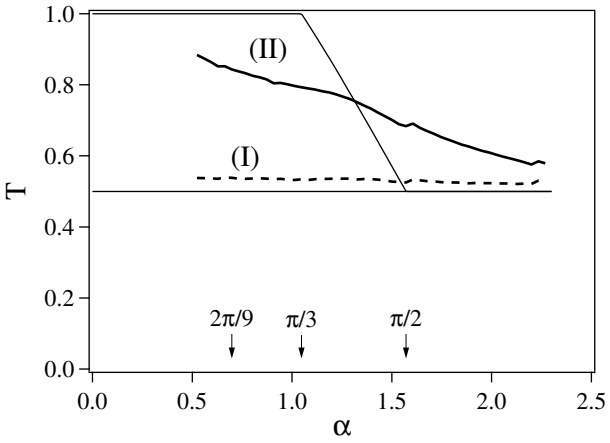

FIG. 4: Transmission rate defined by Eq. (5) versus the summit angle α. The thick dashed and solid lines indicate the transmission rate for case (I) and (II), respectively. The thin lines indicate the transmission rates for (I) and (II) based on the ray acoustics.

hand, the transmission rate of case (I) becomes 0.5, independent of α. For finite wavelength, the transmission rate changes with α as shown in Figs. 2 and 3, showing larger transmission rate at $\alpha = \frac{2\pi}{9}$ than that at $\alpha = \frac{\pi}{3}$. From the comparison and the transmission rate predicted from the ray-acoustics, the rectification effects will decay with increasing α. In order to investigate the angle dependence, we examine the change in the transmission rates for variation of α. Generating a wave packet having a Gaussian spectral distribution of central frequency $\omega_C = \frac{5\pi}{2}\frac{c}{a}$ with $\Delta\omega = \frac{\pi}{2}\frac{c}{a}$, we evaluate the transmission rate for the wave packet, defining

$$T = \frac{\int\int_{\omega_C-\Delta\omega}^{\omega_C+\Delta\omega} \hat{J}_x(\omega) d\omega dy dz}{\int\int_{\omega_C-\Delta\omega}^{\omega_C+\Delta\omega} \hat{J}_x^0(\omega) d\omega dy dz}. \qquad (5)$$

Figure 4 plots the transmission rates defined by Eq. (5) versus α. The difference in the transmission rates decreases with increasing α, however, the rectification effects survive for $\alpha \geq \frac{\pi}{2}$. We also find that the transmission for (I) is slightly larger than 0.5. We may regard these deviations from the prediction based on the ray-acoustics as diffraction effects.

The threshold frequency for the rectification and the periodic change in the transmission rate originate from the interference effects. Because of the periodic structure in the y direction, the scattering is subject to the Bragg diffraction. The reciprocal lattice vector $\mathbf{G}$ given by $\mathbf{G} = (\xi, \frac{n\pi}{a}, 0)$ forms a set of lines in the reciprocal lattice space, where ξ is an arbitrary real number. Because the scattering is elastic, the wave vector of incident wave $\mathbf{k}$ and that of scattered wave $\mathbf{k}'$ satisfy $|\mathbf{k}| = |\mathbf{k}'|$ and the scattering takes place when $\mathbf{k} = \frac{\omega}{c}(1,0,0)$ for (I) and $\mathbf{k} = -\frac{\omega}{c}(1,0,0)$ for (II) satisfies the following diffraction condition $|\mathbf{k}| = |\mathbf{k} + \mathbf{G}|$. In terms of the "Ewald sphere" [9](actually the Ewald circle in the $x-y$ reciprocal space plane in the present system), the wave vectors of scattered waves are indicated by the intersections of the Ewald circle and the lines in the reciprocal lattice space as shown in Fig. 5. The scattered waves have the quantized y-component of wave vector $k_y = \frac{n\pi}{a}$. It is obvious that there is no intersection except for the line with $n = 0$ for $ka < \pi$. On the other hand, the scattered wave for $ka > \pi$ may have a finite k_y. In the former case, the incident waves in the x direction are scattered only forward or backward, even if the waves are scattered from the legs of triangles, resulting in the transmission rates independent of the incident-wave directions. Redirection of the incident waves for scattering takes place only in the latter case because of the finite k_y. The geometry of the scatterers enhances or suppresses the redirection depending on the incident directions of the wave. Hence the rectification takes place only for $ka > \pi$ or $\omega > \frac{c\pi}{a}$.

As readily understood from Fig. 5, the dips in the transmission rates appear when the Ewald circle touches the lines in the reciprocal lattice space. The density of states concerning the scattering diverges in that case, giving rise to large scattering in the y direction. This results in the dips in the transmission rate. We demonstrate the large scattering in the y direction, examining the differential cross section. Supposing a wave impinging on the bottom of triangles in case (I), another wave is generated to satisfy the boundary condition at the surface of holes. The latter wave becomes the scattered wave, which can be approximated in the left region as

$$u = u_C\sqrt{k} \sum_{m=-N/2}^{N/2} \int_{-a/2+2ma}^{a/2+2ma} \frac{e^{ikr}}{\sqrt{r}} d\xi, \qquad (6)$$

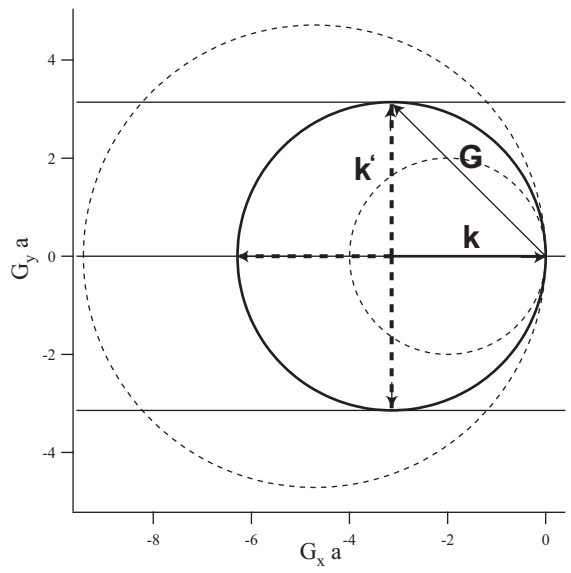

FIG. 5: The Ewald circle (circles in $x-y$ plane) and the reciprocal lattice lines. $\mathbf{k}$ (solid arrow) and $\mathbf{k}'$ (dashed arrows) are the wave vectors of the incident and scattered wavs for the solid circle. These wave vectors are connected by the reciprocal lattice vector $\mathbf{G}$ (thin arrow). Strong scattering takes place in the lateral directions together with forward and backward scattering. Only the forward and backward scattering occur for the smaller dashed circle, on the other hand the waves are scattered in more directions for the larger dashed Ewald circle.

following the Huygens-Fresnel principle[10]. Amplitude u_C is assumed to be the same for all the point sources of scattered waves. The differential cross section yields in the asymptotic field $\frac{r}{a} >> 1$

$$\lim_{N\to\infty} \frac{1}{2Na} r_0 |u|^2 = \pi u_C^2 \, j_0^2 \left(\frac{ka \sin\theta}{2} \right) \frac{1}{\cos\theta} \delta \left(\theta - \sin^{-1} \frac{n\pi}{ka} \right), \tag{7}$$

where r_0 is the distance from the center of the scatterers and θ is an angle from the normal vector of the bases, limited in the region $[-\frac{\pi}{2}, \frac{\pi}{2}]$ (Fig. 1). $j_0(x)$ in Eq. (7) is the first kind of spherical Bessel function of zeroth order. It is obvious from Eq. (7), the differential cross section diverges at $\theta = \pm\frac{\pi}{2}$ and then the waves are scattered in the y direction when $\frac{\omega a}{c} = n\pi$. Otherwise, although the waves are scattered, the scattering rate is not as large as the case of $\frac{\omega a}{c} = n\pi$. Hence the dips in the transmission rates are attributed to the divergence of the differential cross section.

The differential cross section Eq. (7) contains the factor $j_0^2\left(\frac{ak}{2}\sin\theta\right)$, which vanishes for even n. As a consequence, the strong reflection will appear only for the odd n. This is confirmed in Figs. 2 and 3 for case (I). The periodic behavior and the change in the dips are common to case (II). The scattering for case (II) strongly suffers from multiple scattering among the scatterers, and then the simple calculation as done for case (I) is not available, but we confirm numerically the same tendency.

In conclusion, we propose an acoustic-wave rectifier and numerically demonstrate the rectification effects. The rectification is essentially due to the geometric effects of the asymmetric scatterers like the ballistic-particle flows, however, which is remarkably enhanced by the interference among the scattered waves. The threshold frequency for the rectification originates from the periodic structure. Hence, it is possible to tune the rectifier by adjusting the arrangement of the scatterers. The findings of the present work can be applied not only to sound waves in solids or liquids but also in optical waves, leading to new devices in wave engineering. Finally, we mention about the effects of mode conversion occurring at the surface of scatterers on the rectification. In case of the LA and TA waves polarized in the $x-y$ plane, the mode conversion between the waves affects the transmission, however, it is not destructive for the rectification. Preliminary calculations show the transmission rates similar to Figs. 2 and 3 with some modifications due to the mode conversion, which will be discussed elsewhere.

NN acknowledges Franco Nori for fruitful discussion on rectification. RK appreciates the support by the 21st century COE program "Topological Science and Technology" from the Ministry of Education, Culture, Science and Technology of Japan. This work is supported in part by a grant-in-aid for scientific research from the Ministry of Education, Culture, Science and Technology of Japan (Grant No. 1965106507).

* Corresponding author :nn@eng.hokudai.ac.jp

[1] A. M. Song, A. Lorke, A. Kriele, J. P. Kotthaus, W. Wegscheider and M. Bichler, Phys. Rev. Lett. **80**, 3831 (1998).
[2] R. Fleischmann and T. Geisel, Phys. Rev. Lett. **89**, 016804 (2002).
[3] H. Linke, W. Sheng, A. Lofgren, H-G Xu, P. Omling and P.E. Lindelof, Europhys. Lett. **44**, 343 (1998).
[4] D.E. Shalom and H. Pastoriza, Phys. Rev. Lett. **94**, 177001 (2005).
[5] J.E.Villegas, S. Savalev, F. Nori, E.M Gonzalez, J.V Anguita, R.Garcia and J.L Vicent, Science **302**, 1188 (2003).
[6] C. W. Chang, D.Okawa, A. Majumdar and A. Zettl, Science **314**,1121 (2006).
[7] A.Taflove and S.C.Hagness, *Computational Electrodynamics: The Finite-Difference Time-Domain Method*, (Artech House, Boston, MA, 2000).
[8] G.Mur, IEEE Trans. Electromagn. Compat., **23**, 377 (1981).
[9] B. D. Cullity, Elements of X-Ray Diffraction (Addison-Wesley; 1st ed.1957).
[10] M. Born and E. Wolf, Principles of Optics: Electromagnetic Theory of Propagation, Interference and Diffraction of Light, Cambridge Univ Pr (Sd), 1999, Chap.VIII.